Accepted Manuscript

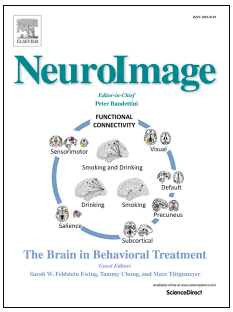

Feasibility of imaging epileptic seizure onset with EIT and depth electrodes

Anna Witkowska-Wrobel, Kirill Aristovich, Mayo Faulkner, James Avery, David Holder

PII: S1053-8119(18)30163-0

DOI: 10.1016/j.neuroimage.2018.02.056

Reference: YNIMG 14757

To appear in: *NeuroImage*

Received Date: 3 November 2017

Revised Date: 22 February 2018

Accepted Date: 26 February 2018

Please cite this article as: Witkowska-Wrobel, A., Aristovich, K., Faulkner, M., Avery, J., Holder, D., Feasibility of imaging epileptic seizure onset with EIT and depth electrodes, *NeuroImage* (2018), doi: 10.1016/j.neuroimage.2018.02.056.

This is a PDF file of an unedited manuscript that has been accepted for publication. As a service to our customers we are providing this early version of the manuscript. The manuscript will undergo copyediting, typesetting, and review of the resulting proof before it is published in its final form. Please note that during the production process errors may be discovered which could affect the content, and all legal disclaimers that apply to the journal pertain.

View metadata, citation and similar papers at core.ac.uk

brought to you by CORE

provided by UCL Discovery

ACCEPTED MANUSCRIPT

Feasibility of imaging epileptic seizure onset with EIT and depth electrodes

Anna Witkowska-Wrobel, Kirill Aristovich, Mayo Faulkner, James Avery and David Holder

Dept. of Medical Physics and Biomedical Engineering, University College London, London WC1E 6BT, United Kingdom

E-mail: anna.wrobel@ucl.ac.uk

Abstract: Imaging ictal and interictal activity with Electrical Impedance Tomography (EIT) using intracranial electrode mats has been demonstrated in animal models of epilepsy. In human epilepsy subjects undergoing presurgical evaluation, depth electrodes are often preferred. The purpose of this work was to evaluate the feasibility of using EIT to localise epileptogenic areas with intracranial electrodes in humans. The accuracy of localisation of the ictal onset zone was evaluated in computer simulations using 9M element FEM models derived from three subjects. 5mm radius perturbations imitating a single seizure onset event were placed in several locations forming two groups: under depth electrode coverage and in the contralateral hemisphere. Simulations were made for impedance changes of 1% expected for neuronal depolarization over milliseconds and 10% for cell swelling over seconds. Reconstructions were compared with EEG source modelling for a radially orientated dipole with respect to the closest EEG recording contact. The best accuracy of EIT was obtained using all depth and 32 scalp electrodes, greater than the equivalent accuracy with EEG inverse source modelling. The localisation error was 5.2±1.8, 4.3±0 and 46.2±25.8mm for perturbations within the volume enclosed by depth electrodes and 29.6±38.7, 26.1±36.2, 54.0±26.2mm for those without (EIT 1%, 10% change, EEG source modelling, n=15 in 3 subjects, $p<0.01$). As EIT was insensitive to source dipole orientation, all 15 perturbations within the volume enclosed by depth electrodes were localised, whereas the standard clinical method of visual inspection of EEG voltages, only localised 8 out of 15 cases. This suggests that adding EIT to SEEG measurements could be beneficial in localising the onset of seizures.

Keywords: EIT, epilepsy, seizure, depth electrodes, imaging

Highlights:

- A new method is proposed to use EIT to localise the area of interictal and ictal activity in patients with implanted depth electrodes.
- The location accuracy was significantly better with the best EIT protocol than with EEG inverse source modelling or SEEG visual inspection in computer simulations.
- EIT was not sensitive to dipole orientation, while EEG detection varied with the field angle demonstrated in modelling.
- A combination of EIT and SEEG can potentially improve the diagnostic yield in epilepsy.

1. Introduction

1.1. Background

Epilepsy is one of the most common chronic neurological diseases (Ngugi, Bottomley, Kleinschmidt, Sander, & Newton, 2010). Patients with focal epilepsy can potentially benefit from resective surgery if

the epileptogenic zone can be clearly identified (Duncan, Sander, Sisodiya, & Walker, 2006) (Regesta & Tanganelli, 1999). To describe this zone precisely, a multidisciplinary assessment is required, which may include prolonged scalp EEG with video telemetry, epilepsy protocol neuroimaging, neuropsychology and neuropsychiatry (NICE, 2016) (Duncan, 2011). The estimated localisation accuracy of scalp EEG is limited to approximately 10-20 mm underneath the electrodes, and decreases significantly for deep sources (Merlet & Gotman, 1999) (Yvert, Bertrand, Thevenet, Echallier, & Pernier, 1997) (Cuffin, Cohen, & Yunokuchi, 1991) (Cohen, et al., 1990).

Improved localisation is offered by intracranial EEG (Benbadis, Wyllie, & Bingaman, 2005), which has the highest spatiotemporal resolution among current clinical methods for seizure monitoring (Schindler, et al., 2016). The main intracranial EEG monitoring methods are subdural grids, strips (ECoG), and depth electrodes (stereo-EEG, SEEG). However, spatial sampling is limited to the cortical region adjacent to the electrodes. The ability to detect a seizure source depends on the distance of the source from the nearest contact. The sampled area for each contact is approximately a 5-mm-radius sphere around the contact boundary (von Ellenrieder, Beltrachini, & Muravchik, 2012) (Lachaux, Rudrauf, & Kahane, 2003). EEG detection also depends on the amplitude of the generator, as well as the orientation of the source, as a dipolar source will not register, if oriented tangentially to electrodes (Burle, et al., 2015) (Ramantani, et al., 2013) (Fisch, 2009) (Lüders, 2008) (Smith, 2005) (Teplan, 2002) (Ebersole, 1997). Out of all invasive intracranial monitoring techniques, depth electrodes have been shown to carry the least risk for patients (Mullin, et al., 2016). Hence, when possible, SEEG has recently been favoured over ECoG (Jayakar, et al., 2016). However, the rates for postsurgical seizure freedom vary between 49% and 83% for temporal lobe epilepsy (de Tisi, et al., 2011) (Murphy, et al., 2010), and 14.7% and 66% in extratemporal lobe epilepsy (McIntosh, et al., 2012) (Jehi, O'Dwyer, Najm, Alexopoulos, & Bingaman, 2009). One reason for early seizure reoccurrence is an incomplete or inaccurate localisation of the onset (Ryvlin & Rheims, 2016). Improvements in the localisation method could yield better patient outcomes.

Electrical Impedance Tomography (EIT) is an imaging technique where 3D images of internal conductivity changes in an object are reconstructed from boundary measurements (Holder, 2005). It has the potential to provide improved localisation of the epileptogenic zone, as seizure activity changes local impedance in two differing ways. These two mechanisms are: 1) "Slow" impedance changes. In epilepsy, slow changes of magnitude up to 12% were detected over 10 seconds after seizure onset in animal models using epicortical electrodes (Wang, Sun, Xu, Dong, & Gao, 2017) (Elazar, Kado, & Adey, 1966) (Adey, Kado, & Didio, 1962) (Van Harreveld & Schade, 1962) and have been imaged with EIT with a ring of electrodes placed on the exposed cortex of a rabbit (Rao, Gibson, & Holder, 1997). These changes are caused by cell swelling and resultant shrinkage of extracellular space during seizures (Lux, Heinemann, & Dietzel, 1985). This is consequent to changes in extracellular potassium ions and water due to intense depolarisation in the area (Niermann, Amiry-Moghaddam, Holthoff, Witte, & Ottersen, 2001). 2) "Fast" impedance changes. Recent work on animals has demonstrated the feasibility of detecting fast impedance decreases of magnitude up to 1% in chemically induced seizures in cortex only using EIT with epicortical electrode arrays in rats (Vongerichten, et al., 2016) (Andrew & MacVicar, 1994). These "fast changes" are due to the opening of ion channels during synchronised neuronal depolarisation (Oh, Gilad, Ghosh, Schuettler, & Holder, 2011) (Klivington & Galambos, 1967). Unfortunately, both types of changes have not yet been successfully imaged by EIT with scalp EEG electrodes: in epileptic patients the expected signal was masked by movement artefacts during seizures, thus the SNR was too low for imaging (Fabrizi, et al., 2006).

Current levels used for EIT meet safety criteria specified in the International Electrotechnical Commission (IEC 60601-1, 2005) and the British Standard Institute (BS5724, 1979). Typically, currents of 50μA at 1.7 kHz are employed in intracranial EIT with epicortical electrodes for imaging of epileptic spikes (Vongerichten, et al., 2016). As the electrode diameter was 1.1 mm, this corresponds to a current density near the electrodes of c. 6.03A/m^2, which rapidly falls off away from the electrodes. Studies indicate current densities up to 250 A/m^2 may be safely injected via intracranial electrodes with no apparent pathological effect on the neural tissue (McCreery, Agnew, Yuen, & Bullara, 1990). Such current levels have no discernible effect on cortical evoked responses (Aristovich, et al., 2016). In this simulation study, similar currents of 50μA were used.

The motivation for this work was the idea that EIT could be used with existing intracranial electrodes placed for SEEG. EIT could be used as a complementary tool to the existing EEG recording equipment on the clinical ward, with no additional risks for the patient. EIT is not sensitive to dipole orientation and could potentially provide better resolution compared to existing clinical methods. However, if only depth electrodes are used, the injected current might be too localised, and hence, the real onset may be missed. We therefore also evaluated the advantages of the concurrent use of scalp electrodes to improve coverage. If successful, the method could reduce the number of depth probes implanted.

Potential applications for EIT in epilepsy clinics could be lateralising the onset, such as mesial temporal lobe onset in patients with bilateral hippocampal abnormalities or differentiating the lobe in patients with fronto-temporal onset in scalp EEG. EIT could aid the localisation of the onset in situations where scalp EEG can be misleading, such as in patients with a previous resection. Finally, identifying the onset in multifocal abnormalities or imaging interictal discharges and their propagation could be a useful tool in clinics.

1.2. Purpose

The purpose of this work was to determine if EIT could offer improved accuracy in localising the seizure onset zone in human subjects with epilepsy that had intracranial electrodes implanted for onset detection. This was examined in computer simulation for both fast and slow impedance changes known to occur during seizures. Specific questions to be addressed were:

1) Which electrode arrangement gives the best seizure onset localisation? Three combinations were assessed: i) intracranial depth electrodes only ii) intracranial electrodes and 32 scalp electrodes iii) a reduced selection of available depth and scalp electrodes with enhanced sensitivity for a defined region of interest.
2) Does the best of these three methods give improved seizure onset detection compared to the current intracranial method with visual inspection of SEEG voltages or EEG inverse source localisation?

1.3. Experimental design

Patient-specific detailed Finite Element Method (FEM) head models were created from combined T1-weighted MRI and high-resolution CT scans for three epilepsy patients (Jehl, Aristovich, Faulkner, & Holder, 2016). The three epilepsy cases considered had 7-12 depth electrodes. Realistic conductivities of head tissues obtained from published literature were used (Malone, Jehl, Arridge, Betcke, & Holder, 2014) (Romsauerova, et al., 2006) (Horesh L. , 2006). Conductivity changes imitating seizure onset were inserted into each mesh. These were spheres, 5 mm in diameter, with -1% or +10% conductivity changes,

representing the “fast” and “slow” impedance changes during seizures respectively (Vongerichten, et al., 2016) (Rao, Gibson, & Holder, 1997) (Elazar, Kado, & Adey, 1966). At least 90% of their elements were in grey matter with the rest being in the white matter that is representative of the real onset zones (Concha, Beaulieu, Collins, & Gross, 2009). The size of the perturbations was chosen as a trade-off between tissue volume, which would realistically proceed to a resective surgery, and offering a more stringent test of the method than perturbations used in previous brain EIT studies. This diameter represents the smallest tissue volume, which would be considered for resection, and involves the destruction of the minimum anatomy important in the pathophysiology during epilepsy surgery. The FEM meshes were used in the forward calculation, while coarser meshes were used for image reconstruction. Images were reconstructed using zeroth order Tikhonov regularization with noise-based image post-processing (Aristovich, dos Santos, Packham, & Holder, 2014). The regularisation hyper parameter was chosen automatically using leave-one-out cross-validation for each reconstruction (for software details see Appendix B).

Three different EIT configurations were simulated: clinically implanted depth electrodes only (Depth Only), a mixture of depth and scalp electrodes (Depth+Scalp) and reduced number of depth and scalp electrodes (ROI-focused). The validity of each EIT protocol was assessed by the location and shape errors of reconstructed conductivity changes in a simulation study.

The EIT results were compared to those obtained using EEG. To investigate the dependence upon the source orientation, in each location, seizure sources were modelled as current dipoles, which were rotated through 190 different solid angles to cover 360□ range. The magnitude of the simulated sources was set such that a voltage of 2mV was produced at an electrode 6mm away, as this is a typical value encountered in clinical practice (Hufnagel, Dumpelmann, Zenter, Schijns, & Elger, 2000). The source detection was evaluated in two different ways. The first was to simulate visual detection of a spike as undertaken by clinicians. A 250μV threshold was set based on an assumption of 100μV peak-to-peak background noise, equivalent to a significance of $p<0.01$, as a reasonable approximation for acceptance visual recognition of a spike against the background signal (Alarcon, 1996). Secondly, image metrics were calculated for EEG source modelling. In this model, the same meshes, conductivities and stabilisation methods were used to calculate lead-field matrices and for image reconstruction in the EEG inverse source modelling.

2. Materials and methods

2.1. Epilepsy cases, mesh creation and seizure onset simulations

The study was based on the datasets obtained from three epileptic patients suffering from prolonged pharmacoresistant focal epilepsy. All patients underwent the procedure of depth electrodes implantation, which was followed by seizure monitoring over days at the Telemetry Ward at the National Hospital for Neurology and Neurosurgery (NHNN), London. In all three cases presented, findings from scalp EEG telemetry suggested frontotemporal epilepsy. There were 7, 11, and 12 depth electrodes implanted, with 48, 82, and 71 recording contacts in total respectively for cases one to three (Figure 1). Although in each case the onset zone was clearly recognised during telemetry, none of the patients proceeded with the resective surgery, due to a possibility of acquiring significant neuropsychological deficits.

Realistic head meshes were segmented from joint T1-weighted MRI and CT scans using open source software (Seg3D, http://www.seg3d.org, 2015, MIPAV, http://mipav.cit.nih.gov/, 2015, CGAL http://www.cgal.org/, 2015, MedInria https://med.inria.fr/, 2015). The segmentation included seven layers: SEEG contacts, grey and white matter, CSF, skull, air and scalp tissues. The segmentation method

implemented was adapted from creating meshes in stroke EIT (Jehl, Aristovich, Faulkner, & Holder, 2016). All meshes contained 0.7 mm size elements, which were refined to 0.3 mm in the vicinity of the electrodes (Aristovich, dos Santos, Packham, & Holder, 2014). The resulting meshes comprised 8.9, 9.1, and 9.6 million tetrahedral elements for patients 1 to 3 respectively (Figure 1). The realistic geometry of depth electrodes was modelled from CT scans. Each electrode contact was 2.4 mm long and 1.1 mm in diameter (Ad-Tech, Spencer Probe depth electrodes). Additional 1 cm diameter scalp electrodes were simulated in two electrode protocols; their location was according to the modified International 10-10 EEG System (Oostenveld & Praamstra, 2001). For the reconstructions, hexahedral meshes with 5 mm elements were created which resulted in 39 000, 36 104, and 35 529 elements for patient 1, 2, and 3 respectively.

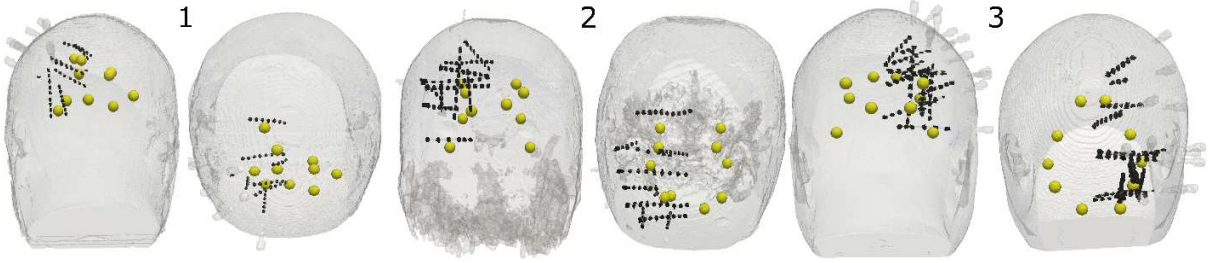

Figure 1. Seizure onset perturbation locations (yellow spheres) inside each mesh with respect to the SEEG depth electrodes and their recording contacts (black dotted lines). Frontal (left) and top of the head view (right) for each patient 1-3.

For EIT simulations, ten seizure onset perturbations were tested (Figure 1): five were located within a volume enclosed by the SEEG contacts (Ipsilateral Group) and the other five placed in the opposite hemisphere, outside the enclosed volume (Contralateral Group). An additional group (Mixed Group) consisted of five perturbations preselected from both groups, Ipsi- and Contralateral. The Mixed Group was proposed to assess the protocol with the reduced number of electrodes (ROI-focused). All perturbations in this group were placed in a line between the current injecting electrodes (depth and scalp).

For EEG modelling, the source was defined as a dipole field generator oriented in the angle most radial with respect to the closest electrode i.e. optimally for source detection.

2.2. Protocols and electrode combinations

Three current injection protocols were tested for EIT simulations. Current injection electrodes were chosen such that the distance between electrodes was maximised, while acquiring the maximum number of independent measurements (Malone, Jehl, Arridge, Betcke, & Holder, 2014). Measurements on all electrodes were taken with respect to a single reference electrode placed in white matter, the same as used for clinical recordings. Across recordings, all available depth contacts were used. These comprised 7 to 12 SEEG electrodes with 48 to 82 contacts, and 32 additional scalp electrodes, placed according to the 10-10 International System (Oostenveld & Praamstra, 2001).

Protocol 1 (‘depth only’): comprised all depth electrodes, which recorded with respect to a reference depth contact used for the SEEG recordings in the clinic. The set combined 48, 82 or 71 contacts, depending on the mesh. There were 47 independent current injections giving 2070 measured voltages, 81

giving 6320, and 70 injections yielding 4692 measurements for cases 1, 2, and 3, respectively. 50μA at 10 kHz was injected.

Protocol 2 ('depth and scalp'): included all depth electrodes and additional 32 scalp electrodes. The forward solution was superimposed on the results from Depth Only protocol, to reduce the processing time. Both sensitivity matrices combined for image reconstruction. There were 31 additional injections between scalp electrodes resulting in 2418, 3472, and 3131 measurement lines, for subjects 1, 2, and 3, respectively. 250μA current was injected between scalp electrodes.

Protocol 3 ('ROI-focused') had a reduced number of current injection sites: three contacts on a single depth electrode (the top, middle and the bottom contact) and less than 10 scalp electrodes on the opposite side of the head, giving up to a maximum total of twelve electrodes. The scalp electrodes were chosen to maximise the current density in perturbation regions. The measurements were made with all available SEEG electrodes. Here, there were 1560, 1680 and 2020 measured voltages for the cases 1, 2, and 3, respectively. The current level was 50 μA. This protocol was used to test, whether a considerably reduced number of injections can still provide useful information on a potential onset, when maximum current density was focused only on a preselected area.

EEG source modelling: all available depth probes and additional 32 scalp electrodes were used in the simulations.

2.3. EIT voltage simulations and image reconstruction

The conductivities were set to: 0.3 S/m for the grey matter, 0.15 S/m for the white matter, 1.79 S/m for the CSF, 0.018 S/m for the skull, 0.44 S/m for the scalp tissues, and 0.0001 S/m for air as specified in the literature for frequencies around 10 kHz (Malone, Jehl, Arridge, Betcke, & Holder, 2014) (Romsauerova, et al., 2006) (Horesh L. , 2006). The conductivity changes inside the seizure onset perturbations were set to 0.003 S/m and 0.03 S/m equivalent to 1% and 10% for the fast and slow impedance changes. The forward solution was calculated using PEITS on the fine tetrahedral meshes (Jehl, et al., 2014). Reconstruction was performed on hexahedral meshes with zeroth order Tikhonov and noise-based image post-processing (Aristovich, dos Santos, Packham, & Holder, 2014). The realistic additive noise of zero mean and a standard deviation of 1μV was added to all simulated voltage changes, which matched the noise in animal experiments with intracranial electrodes (Avery, Dowrick, Faulkner, Goren, & Holder, 2017) (Vongerichten, et al., 2016), resulting in a mean SNR of 22 for 10% changes and 5 for 1% changes.

2.4. EEG source detection

EEG source imaging was accomplished using the same realistic head meshes and conductivity properties of elements as for EIT simulations. The forward lead-field matrix was calculated using the adjoint field theorem and electrical reciprocity principle (Vallaghe, Papadopoulo, & Clerc, 2009) on the tetrahedral head mesh created for all patients. To generate realistic sources, single dipoles were placed in the same 10 locations as the perturbations in the EIT study. The dipoles were represented as spherical perturbations with the same dimensions as for EIT. The elements within the perturbation were assigned a constant current density vector computed on the basis of the detection criterion described by Hufnagel (2000), while the rest of the elements were assigned 0 current density vectors. The voltages were generated on each electrode by multiplication of the lead-field matrix by the resulting current density vector and adding Gaussian random noise with the same parameters as in the EIT case. The source with the most radial (*the max angle*, the highest detected voltage) and the most tangential (*the min angle*, the lowest detected

voltage) orientation were reconstructed into images. These were produced by first computing the inverse source problem solution, then using the resulting electrode voltages combined the lead-field matrix obtained by projection of the forward tetrahedral lead-field matrix into the same hexahedral mesh as used for EIT. Inversion was performed using linear zeroth order Tikhonov regularisation (Grech, et al., 2008), resulting in the current density vector distribution within the entire hexahedral domain. The current density vectors were then weighted using the same noise based t-scoring approach as for EIT for a consistent comparison. Finally, the magnitude of the resulting vectors was used for image display.

2.5. Image quality assessment

The quality of the reconstructed images was evaluated using two metrics: localisation and shape errors (Jehl, Avery, Malone, Holder, & Betcke, 2015) (Malone, Jehl, Arridge, Betcke, & Holder, 2014). The localisation error was defined in millimetres, as the ratio between the distances of the centre of mass of the reconstructed perturbation (at the maximum conductivity change) from the actual location of the perturbation placed within a head mesh. The shape error was defined as the mean of the difference in each axis of the reconstructed perturbation to the perturbation's actual width, expressed as a percentage of the mesh's dimensions. In this case, the reconstructed perturbation contained all voxels with at least 75% (significance defined as 1 standard deviation for 1 degree of freedom Student's t-distribution) of the maximum conductivity change. The average localisation and shape errors were calculated for each of the EIT protocols separately for perturbations from Ipsilateral and Contralateral Groups, and for the EEG sources with the best and the worst source orientation.

The difference between the localisation error for Depth Only and Depth+Scalp protocols in EIT, and Depth+Scalp and EEG source detection were compared with a two-sided t-test, p-value <0.05 or $p<0.01$.

To simulate the clinical procedure of visual inspection for a spike, the generated voltage amplitude for the *max* and the *min* angle of a dipole source were found for each location. This was done to ascertain if the generated voltage was large enough to exceed the 250µV detection threshold on the closest SEEG contact. In order to compare these results with EIT images, an arbitrary clinically acceptable accuracy was set as shape and localisation errors of <10% and 10mm respectively. The comparison was only made with Depth+Scalp Protocol, as this gave the best results of EIT.

3. Results

The Depth and Scalp EIT protocol resulted in better accuracy for both 1% and 10% impedance changes (Figure 2 and Figure 3). For a 1% impedance change, the localisation errors were improved from 26.5±26.8mm to 5.2±1.8mm ($p<0.05$) for the Ipsilateral Group and from 83.1±22.9mm to 29.6±38.7mm ($p<0.01$) for the Contralateral Group, for the Depth Only and Depth+Scalp protocols respectively. Similarly, for a 10% impedance change, the localisation errors were 66.1±37.2mm and 26.1±36.2mm in the Contralateral Group ($p<0.05$). For a 10% ipsilateral change, both protocols resulted in localisation errors of 4.3±0mm. The accuracy of the ROI-focused protocol was severely affected by artefacts (observed especially in the first mesh), which impeded the satisfactory localisation of the seizure onset. There was no significant difference in the shape errors between the Depth Only and Depth+Scalp protocols (Figure 3).

Feasibility of imaging epileptic seizure onset with EIT and depth electrodes

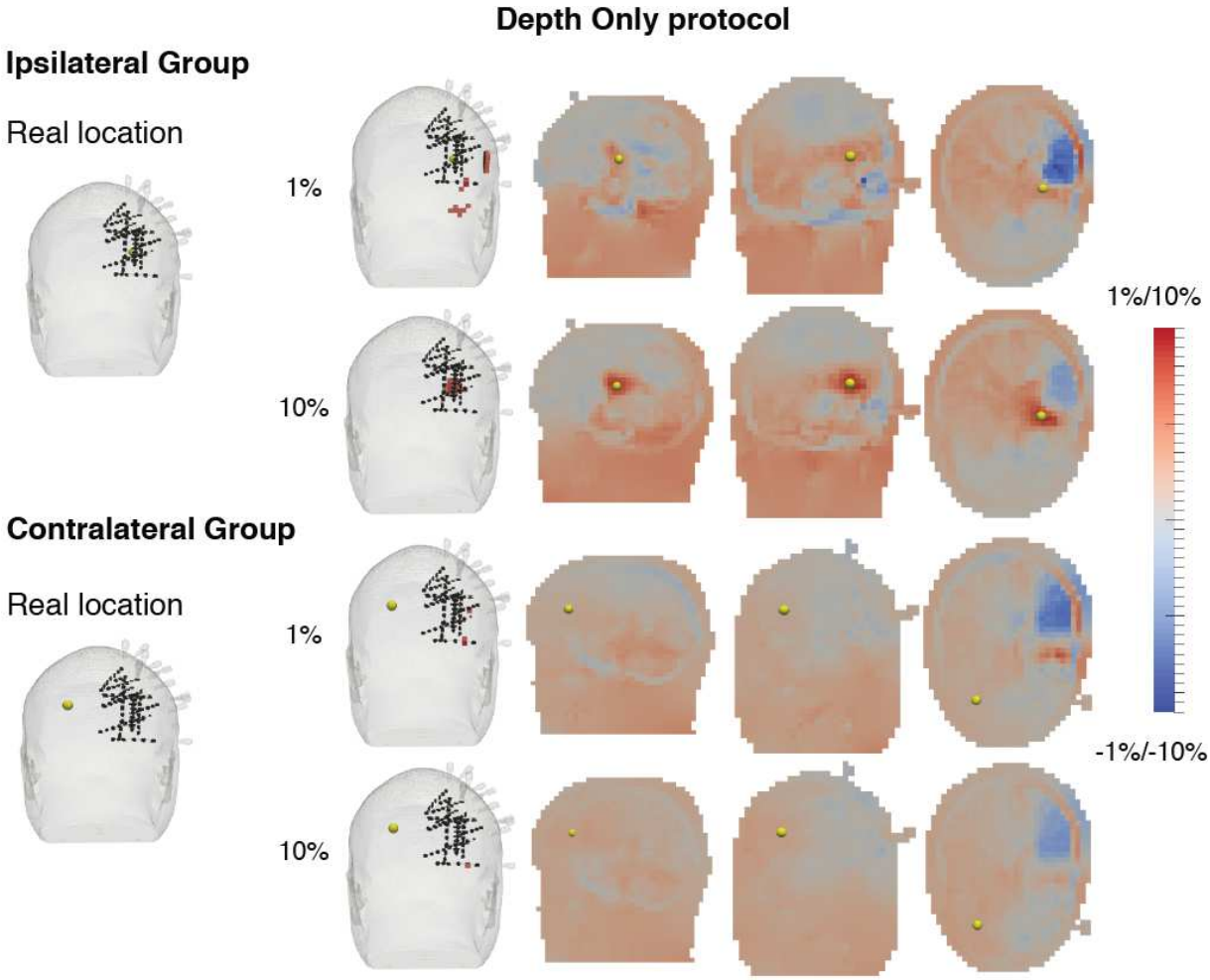

ACCEPTED

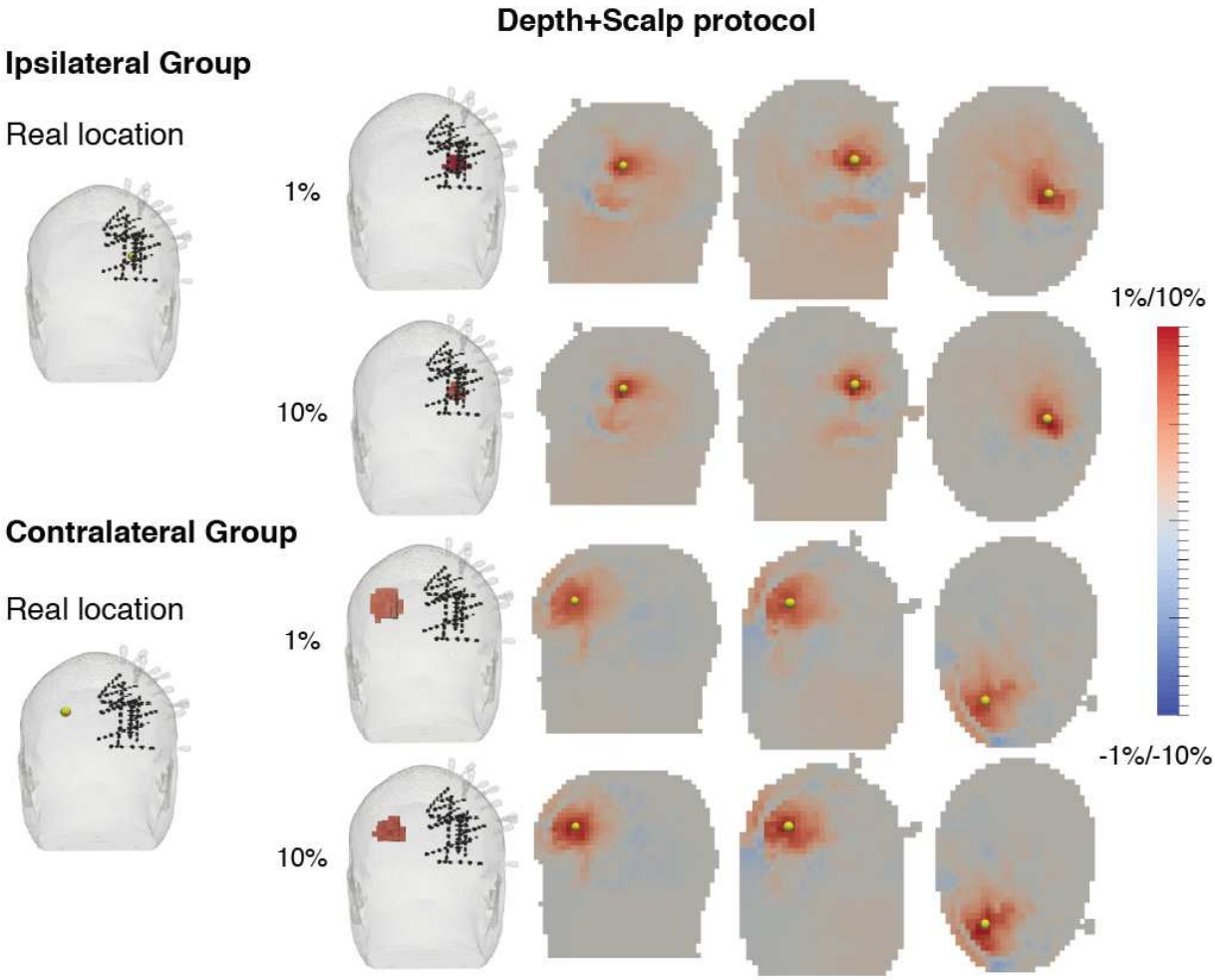
Depth+Scalp protocol
Ipsilateral Group
Real location
1%
10%
Contralateral Group
Real location
1%
10%
1%/10%
-1%/-10%

ACCEPTED

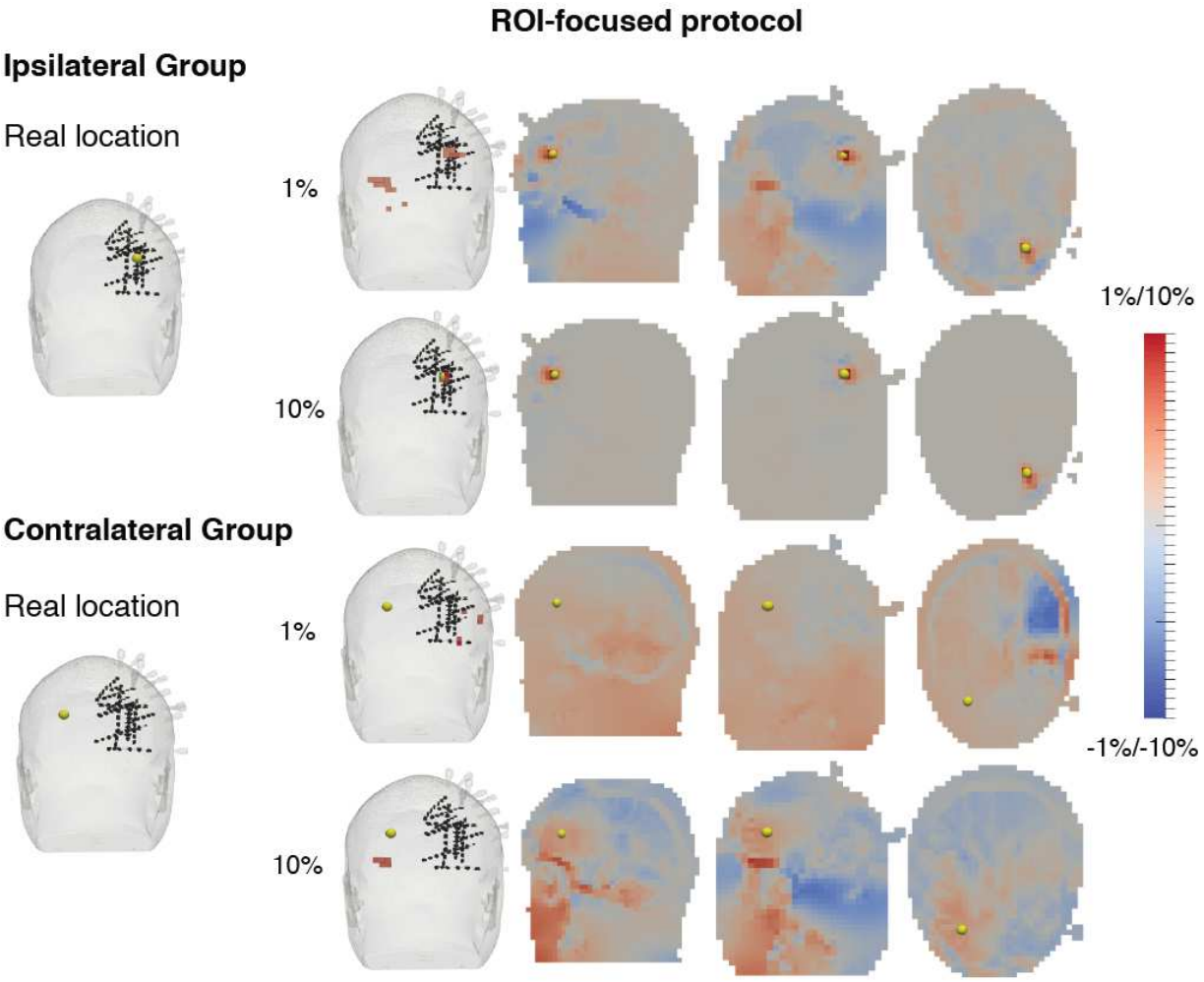

Figure 2. An example of a single perturbation reconstruction; simulations of 1% and 10% impedance changes in both hemispheres for all three protocols tested. The Ipsilateral Group represents perturbations located within SEEG electrodes coverage, the Contralateral Group is in the opposite hemisphere. Each reconstruction is shown in four sections: a front view of a whole mesh with SEEG electrodes and sagittal, coronal, and axial planes. The 'Real location' shows the actual placement of the perturbation (yellow sphere) with respect to the SEEG contacts (black dotted lines). The reconstructed change is presented as a change at 75% threshold of maximum conductivity in the mesh. The scale corresponds to the impedance increase (red) and decrease (blue) in conductivity change (%, t-score based noise correction). It may be seen that the perturbation was reconstructed accurately in all cases for the Depth+Scalp protocol and only for the Ipsilateral Group 10% case for the Depth Only protocol. In case of the ROI-focused protocol, reconstructions were only accurate within close proximity to recording contacts.

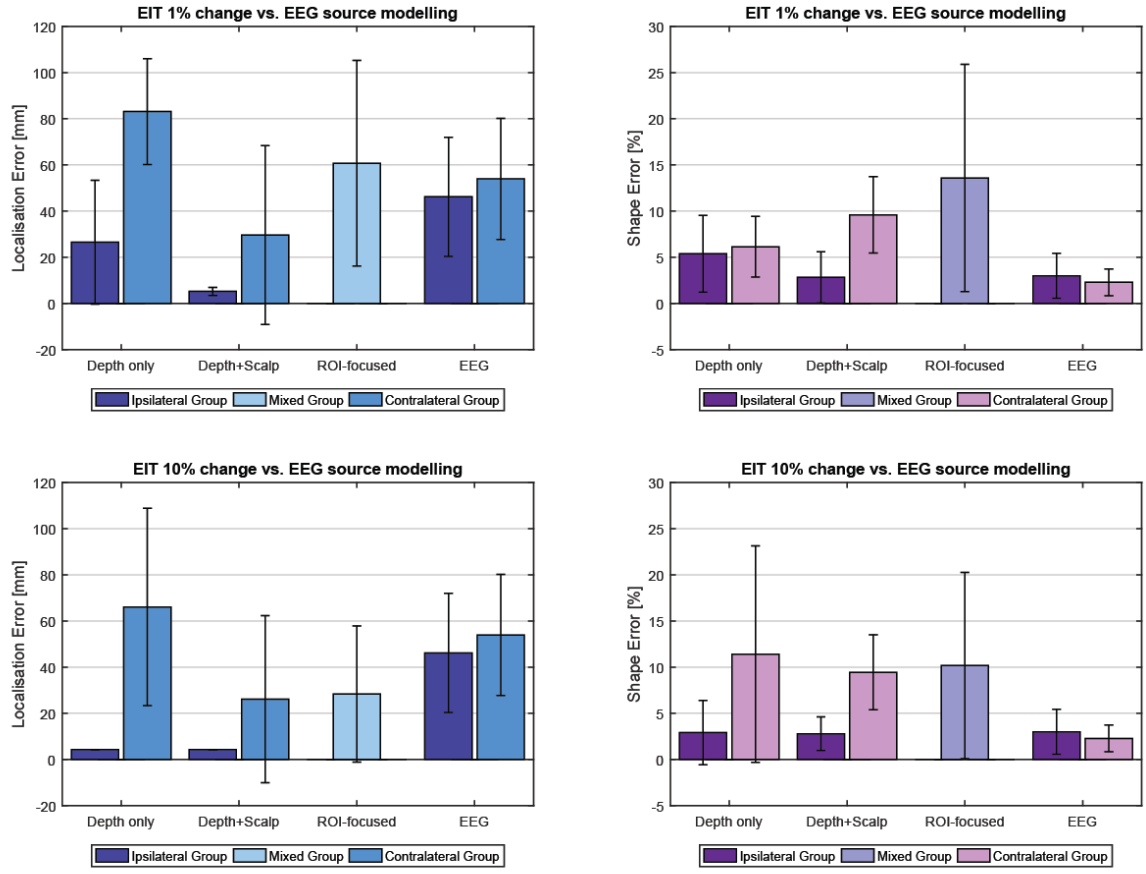

Figure 3. A comparison of the localisation and shape errors with EIT and with EEG source modelling for all the protocols tested in three meshes for fast (1%) and slow (10%) conductivity changes. The Ipsilateral Group represents perturbations placed within the coverage of SEEG electrodes, the Contralateral Group is in the opposite hemisphere, and the Mixed Group is formed from both groups, selected for the ROI-focused protocol. EEG source presents the max angle orientation of the source. Overall, the Depth+Scalp protocol improved the localisation error significantly when compared with the Depth Only protocol (t-test, two-sided, n=15 in each group, details see in Appendix A). For EEG modelling, localisation errors were significantly larger for both groups, Ipsi- and Contralateral, when compared with the EIT Protocol Depth+Scalp. Shape error was improved in the Contralateral Group in EEG.

EEG inverse source modelling resulted in worse localisation accuracy than EIT Depth+Scalp. Localisation errors were 46.2±25.8mm (Ipsilateral Group) and 54.0±26.2mm (Contralateral Group) for the *max* angle, which was significantly worse than with the EIT Depth+Scalp protocol ($p<0.01$ for Ipsilateral Group, $p<0.05$ for Contralateral Group), although the EEG shape error was improved in the Contralateral Group when compared with EIT ($p<0.01$) (Figure 3). The quality of the reconstructed images was considerably better for the *max* angle as opposed to the *min* angle reconstructions (Figure 4); however, it was qualitatively a larger reconstructed region than with EIT.

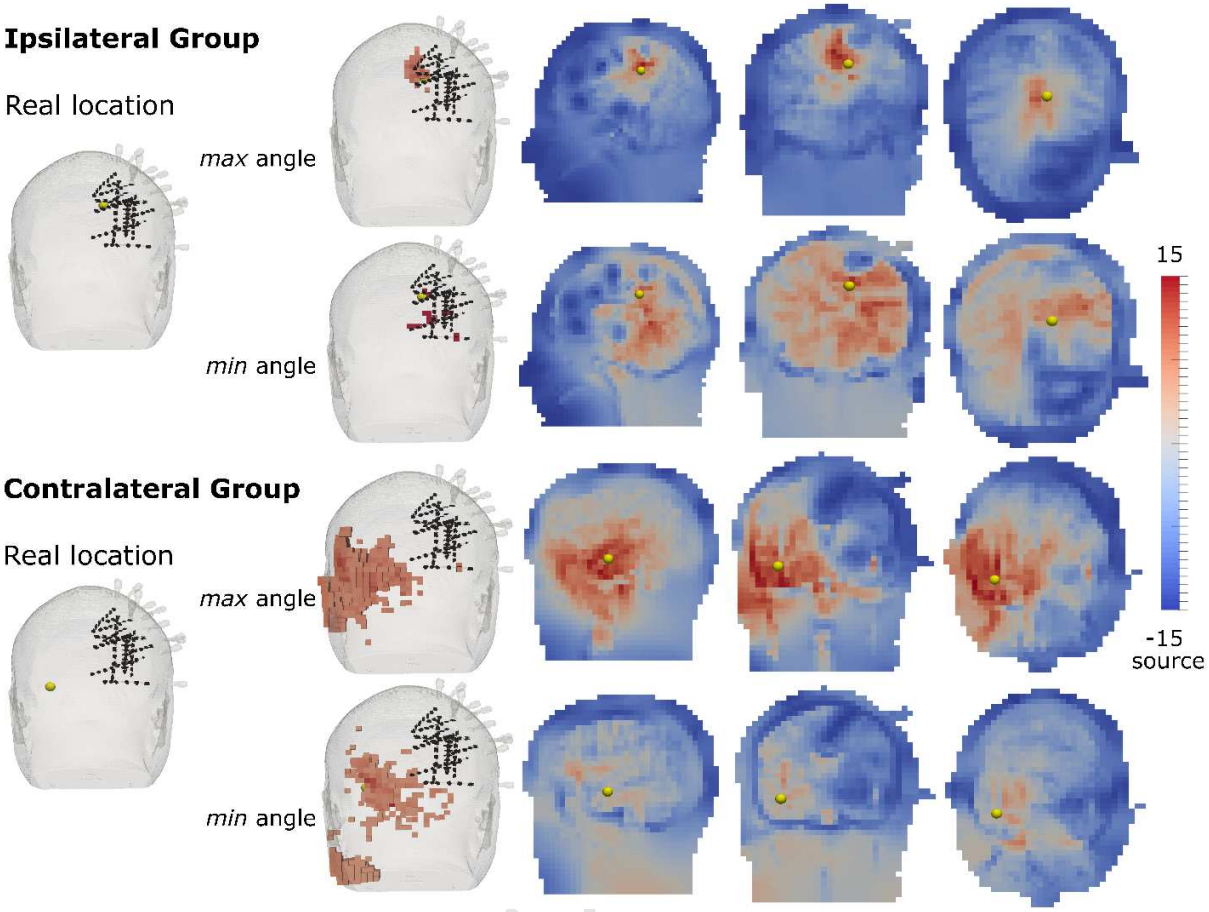

Figure 4. An example of EEG source reconstructions of a single source from the Ipsilateral Group (top panel) and Contralateral Group (bottom panel). For each group, two examples are presented, the reconstruction of the highest voltages detected (the max angle) and the lowest voltages detected (the min angle). Each reconstruction is shown in four sections: a front view of a whole mesh with SEEG electrodes and sagittal, coronal, and axial planes. The 'Real location' shows the actual placement of the perturbation (yellow sphere) with respect to the SEEG contacts (black dotted lines). The reconstructed change is visualised as a change at a 75% threshold of maximum conductivity in the mesh. The scale corresponds to the increase (red) and decrease (blue) in the source signal (source as corrected current density, t-score based noise correction).

With visual spike recognition, 8 out of 15 ipsilateral, and zero contralateral sources generated a field above the detection threshold (Figure 5). In general, sources closer than 11 mm to a contact produced voltages greater than the arbitrary threshold of 250µV and spike amplitude varied with the distance from the recording contact (Figure 6). In contrast, the EIT Depth+Scalp protocol detected 15/15 for both 1 and 10% changes ipsilateral, and 8/15, 9/15 contralateral respectively (Figure 5, top and bottom row, middle and right columns). Spikes were detected up to a maximum distance of 27mm with EIT.

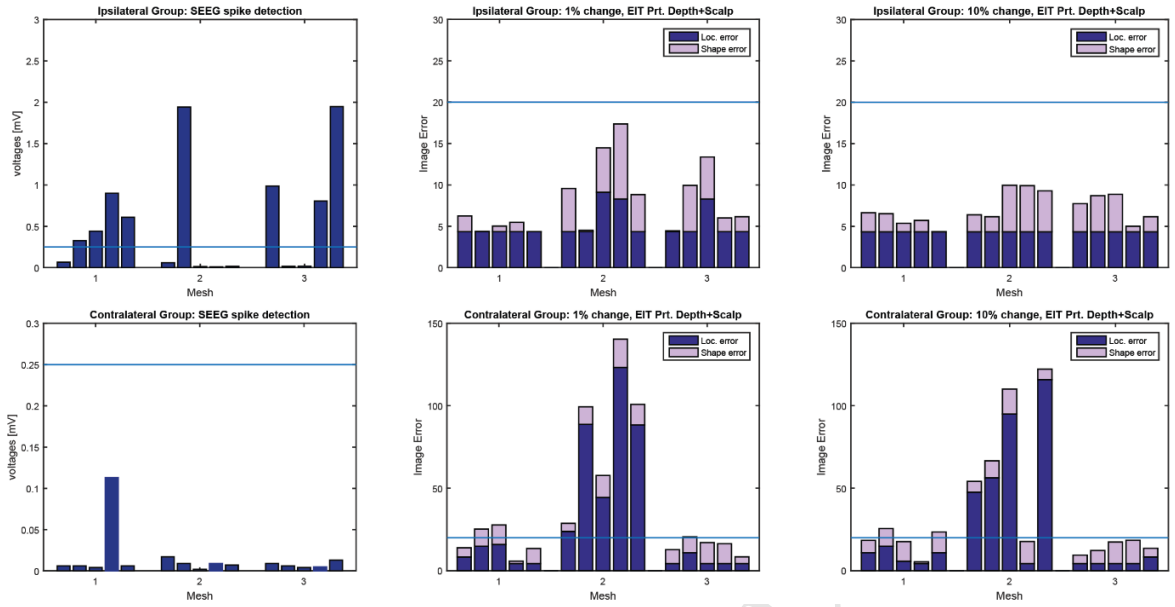

Figure 5. A comparison of the voltages detected on depth electrodes (SEEG spike detection, left column, the max angle) and the combined location and shape errors measured with the EIT Depth+Scalp protocol for the Ipsi- and Contralateral Groups for the 1% (middle column) and 10% (right column) impedance change in all three meshes. The horizontal line represents either a 250µV detection threshold for SEEG spikes or the acceptable combined EIT error (shape and localisation errors of <10% and <10mm respectively).

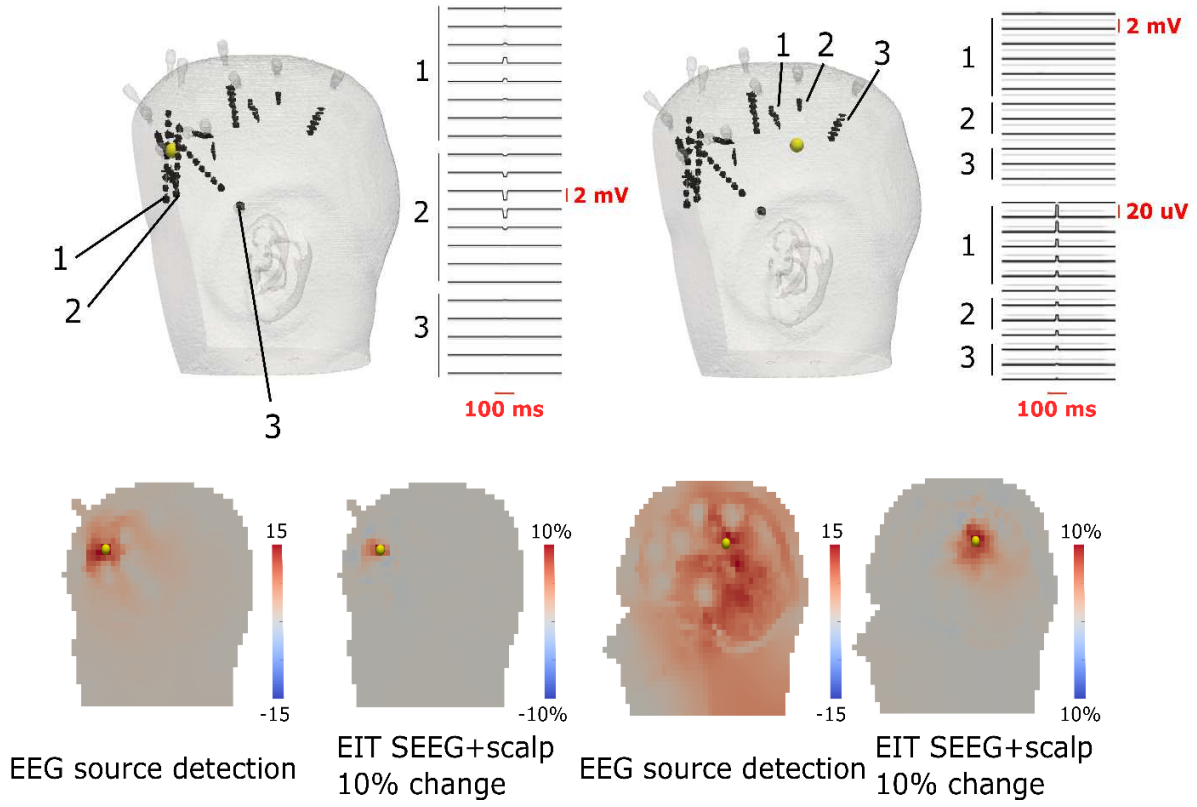

ACCEPTED MANUSCRIPT

Figure 6. Detection accuracy with three methods: the model of clinical spike detection (top, SEEG on respective contacts presented as horizontal lines), the reconstruction with the EEG inverse source (the source as corrected current density, t-score based noise correction) and the best protocol for EIT (Depth+Scalp protocol, described as conductivity change in %, t-score based noise correction) (bottom). The real location of the source is shown as a yellow sphere. Visual detection of a dipole spike shows that sources close to the contact (~7mm distance, left panel) produced spikes above the threshold (the highest amplitude was ~1.5mV) and the spike amplitude changes with respect to the distance and orientation. A more distant source still within SEEG coverage (~18mm distance, right panel) produced a significantly lower voltage (~16μV) on the closest SEEG contact, below the detection threshold of 250μV. In this case, the perturbation was not successfully localised with inverse source modelling but was located within 5mm using EIT.

4. Discussion

4.1. Summary of results

This study demonstrates the feasibility of imaging 1% and 10% conductivity changes with EIT and depth electrodes in computer simulations. EIT resulted in better accuracy than either SEEG spike detection or EEG inverse source modelling and the accuracy of detecting distant and fast impedance changes was further improved when scalp electrodes were added to the protocol.

4.2. Technical issues

The overall computation of the reconstruction procedures for ~9 million tetrahedral- and ~35 000 hexahedral-element meshes involved ~6000 lines of protocol and took up to 240 hours of CPU time for a single patient with the Jacobian matrix taking up to ~500 GB of memory when all depth and scalp electrodes were used. This might raise difficulties in the proposed application of EIT for telemetry and continuous monitoring. However, for each patient, the described method requires only a single time-consuming computation of the forward problem and inverse Jacobian for a given geometry and measurement protocol. It is therefore feasible for prolonged recordings on the ward, as the necessary scaling of the calculations for long-term monitoring is only a matter of simple offline signal processing. Moreover, the time and memory requirements could be reduced by lowering the number of SEEG/EEG contacts for EIT protocol and/or applying coarser meshes, although such modifications would affect the sensitivity of the method. Future work on protocol optimisation in EIT to investigate the minimum required number and locations of depth electrodes for accurate EIT images is in progress.

4.3. Which electrode arrangement gives the best seizure onset localisation?

Three arrangements of electrodes were tested in this study. Among them, the one utilising all depth probes and additional 32 scalp electrodes resulted in the most accurate localisation of the seizure onset.

In clinical practice, it may not always be possible to apply this number of scalp electrodes in a broad 10-20 montage, as there is a potential risk of infection if scalp electrodes were to be located in very close proximity to the craniotomy and burr holes for depth electrodes. Infections are the second main cause of SEEG complications, although they were reported in only 0.8% of patients undergoing depth electrodes implantation and were well controlled with antibiotics (Mullin, et al., 2016). Furthermore, it has not been thoroughly investigated, whether scalp electrodes could affect the risk of infection in clinics. Applying a limited number of scalp electrodes during intracranial monitoring is not a standard clinical procedure but it is sometimes proposed to improve the diagnostic yield. It seems likely that applying scalp electrodes should pose a negligible risk, if scrupulous aseptic technique is used. Ideally, they should be placed

during the same operation as the depth electrodes and with a margin of >2cm from any surgical site. Although these constraints may somewhat reduce the accuracy of the EIT Depth+Scalp protocol described in this study, the use of as many scalp electrodes as possible in safe locations, appears to be a valid recommendation for any future clinical studies.

4.4. Does the best of these three methods give improved seizure onset detection compared to the current intracranial method?

The localisation accuracy was significantly better with the best EIT protocol than with EEG inverse source modelling in the presented models. Also, by its nature EIT was not sensitive to the dipole orientation, whereas EEG detection varied with the field angle and was severely compromised in sub-optimal dipole orientations.

In the presented models, EIT detected the 10%-conductivity-change sources overall better than EEG modelling (Figure 6). Sources placed within 5 mm distance from the electrodes were reconstructed accurately in both EEG inverse source and EIT (Figure 6, left half). When the distance between the perturbation and the nearest recording electrode was extended above 11 mm, the recorded voltage dropped below the EEG detection threshold (Figure 6, right side). Consequently, the inverse source modelling could not accurately locate the source in these instances, while EIT was able to provide reconstructions with an accuracy of 4.3mm.

Imaging the slow 10% impedance changes presented here is likely to be of less clinical impact, as these changes are likely representative of the propagation of the seizure and could be detected through other methods such as EEG-fMRI or SPECT. Nevertheless, this might still be of value in locating the seizure onset zone. Future work should focus on detection of the fast, 1% changes, as they have the highest clinical utility, and are the most challenging to detect with existing methods due to their low SNR and short time course.

There are several further considerations when reconstructing seizure-related changes with EIT. The inverse problem in EIT is ill-posed and ill-conditioned; therefore, it is crucial to minimise modelling errors in the forward problem. In this modelling study, the component head tissues were treated as isotropic and homogenous. This appeared to be reasonably valid in this study, as the brains of the patients showed no observable abnormalities in neuroimaging. In some cases of epilepsy, there could be a local pathology which could influence local tissue impedance. In such cases, the assumption of homogenous conductivity values across the brain tissues should be modified. Such lesions, though, could be visualised in MRI prior to the SEEG implantation and built into the mesh as a separate layer with a different conductivity value. The same procedure can be applied to various post-operative tissue abnormalities following the implantation of electrodes such as haemorrhages, infarcts, oedemas, etc., which can be easily visualised in post-operative CT imaging (Schmidt, et al., 2016). Furthermore, it was recently reported by Koessler et al. (2017) that non-lesional epileptogenic zones can have different conductivity values than the surrounding healthy tissue. Even in such cases, time-difference EIT minimises the impact of such aberrant impedances, as modelling errors are attenuated when the difference between two time points is taken (Holder, 2005) and hence, it may still be possible to achieve acceptable source localisation.

Finally, it is important to note that this study represents only a subset of cases, and therefore it is limited to unilateral intracranial electrode coverage. However, it will be beneficial to extend the method to study cases with bilateral electrode placement, as it may offer some insight into seizure progression from deep onset to cortical regions.

4.5. Conclusions

The feasibility of a new method of combining Electrical Impedance Tomography with depth electrodes implanted for clinical monitoring prior to resective surgery in epilepsy was tested in computer simulations. EIT improved the onset localisation accuracy compared to EEG inverse source modelling and was sensitive to sources not visible with visual spike detection. Future work should focus on detecting fast changes, as these are crucial for the clinical utility of EIT, while slow changes are more likely to be imaged by other methods. Investigating regional limitations to particular cortical or subcortical areas would be similarly beneficial for the development of the method. Furthermore, a rigorous investigation of the relation between the number of depth electrodes and the accuracy of source localisation would demonstrate if EIT has the potential to reduce the number of SEEG electrodes implanted in the future.

The presented results suggest that EIT could aid epilepsy diagnosis when combined with existing methods. Most importantly, EIT could assist in clarifying the location of a seizure onset, if other methods, such as extracranial and intracranial localisation and imaging data, remain unclear. Hence, a combination of EIT and EEG could improve the diagnostic yield and help in better understanding epilepsy, with no additional costs or risks for patients.

Appendix A. Tables

The details on EIT and EEG source modelling image accuracy presented as bar charts in the manuscript are presented below.

Table A1. Results for EIT simulation study: a comparison of the localisation and shape errors for all the protocols tested specified in each mesh and the overall score for both fast (1%) and slow (10%) EIT changes. The Depth+Scalp protocol improved the localisation error significantly, when compared with the Depth Only protocol (t-test, two-sided, $p<0.01$ (**), $p<0.05$ (*), n=15 in each group).

EIT 1% change	Localisation error [mm] (mean ± SD)				
	Prt. Depth Only		Prt. Depth+Scalp		ROI-focused
	Ipsilateral	Contralateral	Ipsilateral	Contralateral	Mixed
Mesh 1	14.3±22.2	60.1±15.3	4.3±0	73.7±39.5	97.2±8.6
Mesh 2	43.6±27.4	107.5±14.1	6.07±2.4	9.5±5.6	36.5±37.9
Mesh 3	21.6±26.3	80.9±6.7	5.1±1.8	5.6±2.9	39.4±53.0
Overall	**26.5±26.8**	**83.1±22.9**	**5.2±1.8(*)**	**29.6±38.7(**)**	**60.7±44.6**

EIT 1% change	Shape error [%] (mean ± SD)				
	Prt. Depth Only		Prt. Depth+Scalp		ROI-focused
	Ipsilateral	Contralateral	Ipsilateral	Contralateral	Mixed
Mesh 1	5.0±3.1	4.0±2.1	0.8±0.8	7.7±4.2	26.4±1.9
Mesh 2	8.6±4.9	10.0±2.1	4.9±3.2	11.7±4.5	2.5±1.8
Mesh 3	2.5±1.7	4.4±0.9	2.9±2.4	9.4±3.5	8.7±11.4
Overall	**5.4±4.1(*)**	**6.1±3.3**	**2.9±2.7**	**9.6±4.1(*)**	**13.6±12.3**

EIT 10% change	Localisation error [mm] (mean ± SD)				
	Prt. Depth Only		Prt. Depth+Scalp		ROI-focused
	Ipsilateral	Contralateral	Ipsilateral	Contralateral	Mixed
Mesh 1	4.3±0	36.0±34.9	4.3±0	63.8±43.4	57.2±27.7
Mesh 2	4.3±0	95.6±41.4	4.3±0	9.3±4.3	7.9±4.9
Mesh 3	4.3±0	66.6±35.3	4.3±0	5.1±1.8	12.7±12.7
Overall	**4.3±0**	**66.1±42.8**	**4.3±0**	**26.1±36.2 (*)**	**28.4±29.5**

EIT 10% change	Shape error [%] (mean ± SD)				
	Prt. Depth Only		Prt. Depth+Scalp		ROI-focused
	Ipsilateral	Contralateral	Ipsilateral	Contralateral	Mixed
Mesh 1	0.9±0.9	15.6±19.1	1.4±0.9	8.8±4.7	19.8±10.2
Mesh 2	4.2±4.8	9.1±1.4	4.0±1.9	10.4±4	4.8±3.9
Mesh 3	3.7±3.5	9.5±9.1	3.0±1.7	9.2±4.2	3.5±0.4
Overall	**2.9±3.5**	**11.4±11.7**	**2.8±1.8**	**9.4±4.1**	**10.2±10.1**

Table A2. EEG source modelling results for the *max* angle of the source. The localisation errors were significantly larger for both groups, Ipsi- and Contralateral, when compared with the EIT Depth+Scalp protocol ((*) $p<0.05$, (**) $p<0.01$). The shape error of the EEG source modelling was overall more significantly improved in the Contralateral Group than in the EIT Depth+Scalp protocol, with an exception the first mesh, in which EIT resulted in a better shape error.

Max angle EEG source imaging	**Localisation error [mm]**		**Shape error [%]**	
	Ipsilateral	Contralateral	Ipsilateral	Contralateral
Mesh 1	35.7±12.4	58.9±20.3	6.2±0.6	3.7±1.4
Mesh 2	35.7±9.6	64.4±37.2	1.9±1.1	1.6±1.2
Mesh 3	67.2±35.6	38.5±12.0	0.9±0.3	1.6±0.7
Overall	**46.2±25.8 (**)**	**54.0±26.2 (*)**	**3.0±2.4**	**2.3±1.4 (**)**

Appendix B. Software Resources

All of the software is released under a GNU General Public License v3.0.

The forward solver is available at https://github.com/EIT-team/ PEITS, and the software for reconstruction is available at https://github.com/EIT-team/Reconstruction.

Acknowledgements

The authors are grateful to Dr. Beate Diehl and Dr. Michele Rizzi from the National Hospital for Neurology and Neurosurgery, Queen Square, University College London NHS Foundation Trust for providing anonymised patient MRI and CT scans from which the FEM models were generated.

This work was supported by DARPA grant N66001-16-2-4066, Blackrock Microsystems and the EPSRC EP/M506448/1.

Conflicts of interest: none

References

Adey, W. R., Kado, R. T., & Didio, J. (1962). Impedance measurements in the brain tissue of chronic animals using microvolts signal. *Exp. Neurol.* , 47-66.

Alarcon, G. (1996). Electrophysiological aspects of interictal and ictal activity in human partial epilepsy. *Seizure*, 7-33.

Andrew, R. D., & MacVicar, B. A. (1994). Imaging cell volume changes and neuronal excitation in the hippocampal slice. *Neuroscience, 62*, 371-383.

Aristovich, K. Y., dos Santos, G. S., Packham, B. C., & Holder, D. S. (2014). A method for reconstructing tomographic images of evoked neural activity with electrical impedance tomography using intracranial planar arrays. *Physiological Measurement, 35(6)*, 1095 - 1109.

Aristovich, K., Packham, B., Koo, H., Santos, G., McEvoy, A., & Holder, D. (2016). , McEvoy, A., & Holder, D. S. Imaging fast electrical activity in the brain with electrical impedance tomography. *NeuroImage*, 204–213.

Avery, J., Dowrick, T., Faulkner, M., Goren, N., & Holder, D. (2017). A Versatile and Reproducible Multi-Frequency Electrical Impedance Tomography System. *Sensor, 17(2)*, 280-300.

Benbadis, S., Wyllie, E., & Bingaman, W. E. (2005). Intracranial Electroencephalography and Localisation Studies. In E. Wyllie, G. D. Cascino, & B. E. Gidal, *Wyllie's Treatment of Epilepsy: Principles and Practice* (pp. 1059-1068).

BS5724. (1979). *Medical electrical equipment. General requirements for basic safety and essential performance.*

Burle, B., Spieser, L., Roger, C., Casini, L., Hasbroucq, T., & Vidal, F. (2015). Spatial and temporal resolutions of EEG: Is it really black and white? A scalp current density view. *International Journal of Psychophysiology, 97(3)*, 210–220.

Cohen, D., Cuffin, B. N., Yonokuchi, K., Maniewski, R., Purcell, C., Cosgrove, G., . . . Schomer, D. L. (1990). . MEG versus EEG localization test using implanted sources in the human brain. . *Ann. Neurol*, 811-817.

Concha, L., Beaulieu, C., Collins, D. L., & Gross, D. W. (2009). White-matter diffusion abnormalities in temporal-lobe epilepsy with and without mesial temporal sclerosis. *J Neurol Neurosurg Psychiatry, 80(3)*, 312–319.

Cuffin, B., Cohen, D., & Yunokuchi, K. (1991). Test of EEG localization accuracy using implanted sources in the human brain. *Ann. Neurol.*, 132-138.

de Tisi, J., Bell, G. S., Peacock, J. L., McEvoy, A. W., Harkness, W., Sander, J., & Duncan, J. S. (2011). The long-term outcome of adult epilepsy surgery , patterns of seizure remission , and relapse : a cohort study. *The Lancet*, pp. 1388-1395.

Duncan, J. S. (2011). Selecting patients for epilepsy surgery: Synthesis of data. . *Epilepsy and Behavior, 20(2)*, 230–232.

Duncan, J. S., Sander, J. W., Sisodiya, S. M., & Walker, M. C. (2006). Adult epilepsy. *Lancet, 367(9516)*, 1087–1100.

Ebersole, J. S. (1997). Defining epileptogenic foci: past, present, future. *Clinical Neurophysiology*, pp. 470-83.

Elazar, Z., Kado, R. T., & Adey, W. R. (1966). Impedance changes during epileptic seizures. . *Epilepsia, 7(4)*, 291–307.

Fabrizi, L., Sparkes, M., Horesh, L., Perez-Juste Abascal, J. F., McEwan, A., Bayford, R. H., . . . Holder, D. S. (2006). Factors limiting the application of electrical impedance tomography for identification of regional conductivity changes using scalp electrodes during epileptic seizures in humans. *Physiological measurement, 27(5)*, S163-S174.

Fisch, B. J. (2009). *Epilepsy and Intensive Care Monitoring: Principles and Practice.* New York, USA: Demos Medical Publishing.

Grech, R., Cassar, T., Muscat, J., Camilleri , K., Fabri, S., Zervakis, M., . . . Vanrumste, B. (2008). Review on solving the inverse problem in EEG source analysis. *J Neuroeng Rehabil*, 5-25.

Holder, D. S. (2005). *Electrical Impedance Tomography: methods, history and applications.* (1st ed.). Francis & Taylor.

Horesh, L. (2006). *Some novel approaches in modelling and image reconstruction for multi frequency electrical impedance tomography of the human brain* (PhD Thesis ed.). University College London.

Hufnagel, A., Dumpelmann, M., Zenter, J., Schijns, O., & Elger, C. (2000). Clinical Relevance of Quantified Intracranial Interictal Spike Activity in Presurgical Evaluation of Epilepsy. *Epilepsia*, 467-478.

IEC 60601-1. (2005). *Medical Electrical Equipment - Part 1: General Requirements for Basic Safety and Essential Performance.* International Standard.

Jayakar, P., Gotman, J., Harvey, A. S., Palmini, A., Tassi, L., Schomer, D., . . . Kahane, P. (2016). Diagnostic utility of invasive EEG for epilepsy surgery: Indications, modalities, and techniques. *Epilepsia, 57(11)*, 1735-1747.

Jehi, L., O'Dwyer, R., Najm, I., Alexopoulos, A., & Bingaman, W. (2009). A longitudinal study of surgical outcome and its determinants following posterior cortex epilepsy surgery. *Epilepsia, 50*, 2040 - 2052.

Jehl, M., Dedner, A., Betcke, T., Aristovich, K., Klofkorn, R., & Holder , D. (2014). A Fast Parallel Solver for the Forward Problem in Electrical Impedance Tomography. *IEEE Transactions on Bio-Medical Engineering, PP(99)*.

Jehl, M., Avery, J., Malone, E., Holder, D., & Betcke, T. (2015). Correcting electrode modelling errors in EIT on realistic 3D head models. *Physiol. Meas., 36*, 2426-2442.

Jehl, M., Aristovich, K., Faulkner, M., & Holder, D. S. (2016). Are Patient Specific Meshes Required for EIT Head Imaging? *Physiological Measurements, 37(6)*, 879–892.

Klivington, K. A., & Galambos, R. (1967). Resistance shifts accompanying the evoked cortical response in the cat. *Science, 157(3785)*, 211-3.

Koessler, L., Colnat-Coulbois, S., Cecchin, T., Hofmanis, J., Dmochowski, J., Norcia, A., & Maillard, L. (2017). In-Vivo Measurements of Human Brain Tissue Conductivity Using Focal Electrical Current Injection Through Intracerebral Multicontact Electrodes. *Human Brain Mapping*, 974-986.

Lachaux, J. P., Rudrauf, D., & Kahane, P. (2003). Intracranial EEG and human brain mapping. *J Physiol, 97*, 613-628.

Lüders, H. (2008). *Textbook of epilepsy surgery.* London: Informa Healthcare.

Lux, H., Heinemann, U., & Dietzel, I. (1985). Ionic changes and alterations in the size of the extracellular space during epileptic activity. *Adv. Neurol., 44*, 619–639.

Malone, E., Jehl, M., Arridge, S., Betcke, T., & Holder, D. (2014). Stroke type differentiation using spectrally constrained multifrequency EIT: evaluation of feasibility in a realistic head model. *Physiological Measurements*, 1051-66.

McCreery, D. B., Agnew, W. F., Yuen, T. H., & Bullara, L. (1990). Charge density and charge per phase as cofactors in neural injury induced by electrical stimulation. *IEEE Transactions on Biomedical Engineering, 37(10)*, 996–1001.

McIntosh, A., Averill, C., Kalnins, R., Mitchell, L., Fabinyi, G., Jackson, G., & Berkovic, S. (2012). Long-term seizure outcome and risk factors for recurrence after extratemporal epilepsy surgery. *Epilepsia, 53*, 970–978.

Merlet, I., & Gotman, J. (1999). Reliability of dipole models of epileptic spikes. *Clinical Neurophysiology, 110(6)*, 1013–1028.

Mullin, J., Shriver, M., Alomar, S., Najm , I., Bulacio, J., Chauvel, P., & Gonzalez-Martinez, J. (2016). Is SEEG safe ? A systematic review and meta-analysis of stereo-electroencephalography – related complications. *Epilepsia, 57(3)*, 386–401.

Murphy, M., Smith, P., Wood , M., Bowden, S., O'Brien, T., Bulluss, K., & Cook, M. (2010). Surgery for temporal lobe epilepsy associated with mesial temporal sclerosis in the older patient: a long-term follow-up. *Epilepsia, 51*, 1024–1029.

Ngugi, A. K., Bottomley, C., Kleinschmidt, I., Sander, J. W., & Newton, C. R. (2010). Estimation of the burden of active and life-time epilepsy: A meta-analytic approach. *Epilepsia, 51(5)*, 883–890.

NICE. (2016). Epilepsies: diagnosis and management.

Niermann, H., Amiry-Moghaddam, M., Holthoff, K., Witte, O., & Ottersen, O. P. (2001). A novel role of vasopressin in the brain: modulation of activity-dependent water flux in the neocortex. *J Neurosci, 21(9)*, 3045-3051.

Oh, T., Gilad, O., Ghosh, A., Schuettler, M., & Holder, D. (2011). A novel method for recording neuronal depolarization with recording at 125-825 Hz: implications for imaging fast neural activity in the brain with electrical impedance tomography. *Med. Biol. Eng. Comput., 49(5)*, 593-604.

Oostenveld, R., & Praamstra, P. (2001). The five percent electrode system for high-resolution EEG and ERP measurements. *Clinical Neurophysiology, 12*, 713-719.

Ramantani, G., Cosandier-Rimélé, D., Schulze-Bonhage, A., Maillard, L., Zentner, J., & Dümpelmann, M. (2013). Source reconstruction based on subdural EEG recordings adds to the presurgical evaluation in refractory frontal lobe epilepsy. *Clinical Neurophysiology, 124(3)*, 481-491.

Rao, A., Gibson, A., & Holder, D. S. (1997). EIT images of electrically induced epileptic activity in anaesthetised rabbits. *Medical and Biological Engineering and Computing, 35(Supplement 1)*, 327.

Regesta, G., & Tanganelli, P. (1999). Clinical aspects and biological bases of drug-resistant epilepsies. *Epilepsy Res., 43(2)*, 109–122.

Romsauerova, A., McEwan, A., Horesh, L., Yerworth, R., Bayford, R., & Holder, D. (2006). Multi-frequency electrical impedance tomography (EIT) of the adult human head: initial findings in

brain tumours, arteriovenous malformations and chronic stroke, development of an analysis method and calibration. *Physiol Meas*, 147-161.

Ryvlin, P., & Rheims, S. (2016). Predicting epilepsy surgery outcome. *Current Opinion in Neurology,, 29(2)*, 182–188.

Schindler, K., Rummel, C., Andrzejak, R. G., Goodfellow, M., Zubler, F., Abela, E., . . . Gast, H. (2016). Ictal time-irreversible intracranial EEG signals as markers of the epileptogenic zone. *Clinical Neurophysiology, 127(9)*, 3051–3058.

Schmidt, R., Wu, C., Lang, M., Soni, P., Williams, K., Boorman, D., . . . Sharan, A. (2016). Complications of subdural and depth electrodes in 269 patients undergoing 317 procedures for invasive monitoring in epilepsy. *Epilepsia*, 1697–1708.

Smith, S. J. (2005). EEG in the diagnosis, classification, and management of patients with epilepsy. . *Journal of Neurology, Neurosurgery, and Psychiatry, 76 Suppl 2*, ii2–7.

Teplan, M. (2002). Fundamentals of EEG measurement. . *Measurement Science Review, 2*, 1–11.

Vallaghe, S., Papadopoulo, T., & Clerc, M. (2009). The adjoint method for general EEG and MEG sensor-based lead field equations. *Phys. Med. Biol.*, 135-147.

Van Harreveld, A., & Schade, J. P. (1962). Changes in the electrical conductivity of cerebral cortex during seizure activity. *Experimental neurology, 400*, 383-400.

von Ellenrieder, N., Beltrachini, L., & Muravchik, C. H. (2012). Electrode and brain modelling in stereo-EEG. *Clin Neurophysiol, 123*, 1745-1754.

Vongerichten, A. N., Santos , G., Aristovich, K., Avery, J., McEvoy, A., Walker, M., & Holder, D. S. (2016). Characterisation and imaging of cortical impedance changes during interictal and ictal activity in the anaesthetised rat. *NeuroImage, 124*, 813-823.

Wang, L., Sun, Y., Xu, X., Dong, X., & Gao, F. (2017). Real-time imaging of epileptic seizures in rats using electrical impedance tomography. *NeuroReport, 28*, 689–693.

Yvert, B., Bertrand, O., Thevenet, M., Echallier, J. F., & Pernier, J. (1997). A systematic evaluation of the spherical model accuracy in EEG dipole localization. *Electroenceph clin Neurophysiol*, 452-459.

ACCEPTED MANUSCRIPT